Synthesis and Self-Assembly of UV-Cross-Linkable Amphiphilic Polyoxazoline Block Copolymers: Importance of Multitechnique Characterization

Kedafi Belkhir, Orélia Cerlati, Diana Heaugwane, Alice Tosi, Tarek Benkhaled, Pierre-Louis Brient, Camille Chatard, Alain Graillot, Sylvain Catrouillet, Stéphanie Balor, et al.

Synthesis and self-assembly of UV-crosslinkable amphiphilic polyoxazoline block copolymers : importance of multi-technique characterization

Kedafi Belkhir[1], Orélia Cerlati[2], Diana Heaugwane[2], Alice Tosi[2], Belkacem Tarek Benkhaled[1], Pierre-Louis Brient[3], Camille Chatard[3], Alain Graillot[3], Sylvain Catrouillet[2], Stéphanie Balor[4], Dominique Goudounèche[5], Bruno Payré[5], Pascale Laborie[6], Jia-Hui Lim[7], Jean-Luc Putaux[7], Patricia Vicendo[2], Laure Gibot[2], Barbara Lonetti[2], Anne-Françoise Mingotaud[2,], Vincent Lapinte[1,*]*

1 ICGM, Université de Montpellier, CNRS, ENSCM, Montpellier, France

2 Laboratoire des IMRCP, Université de Toulouse, CNRS UMR 5623, Université Toulouse III - Paul Sabatier, 118 Rte de Narbonne, 31062 Toulouse cedex 9, France

3 Specific Polymers, 150 Avenue des Cocardières, 34160 Castries, France

4 METi platform, Université Paul Sabatier, 118 route de Narbonne, 31062 Toulouse cedex, France

5 CMEAB Université Toulouse III – Paul Sabatier, 133 Route de Narbonne 31062 Toulouse cedex, France

6 Technopolym, Institut de Chimie de Toulouse ICT-UAR 2599, Université Toulouse 3 – Paul Sabatier, 118 route de Narbonne, 31062 Toulouse cedex 9, France

7 Univ. Grenoble Alpes, CNRS, CERMAV, F-38000 Grenoble, France

KEYWORDS. Amphiphilic polymers, photosensitive polymers, polymeric nanoparticles

ABSTRACT. In the nanomedicine field, there is a need to widen the availability of nanovectors to compensate for the increasingly reported side-effects of poly(ethene glycol). Nanovectors enabling crosslinking can further optimize drug delivery. Crosslinkable polyoxazolines are therefore relevant candidates to address these two points. Here we present the synthesis of coumarin-functionalized poly(2-alkyl-2-oxazoline) block copolymers, namely, poly(2-methyl-2-oxazoline)-*block*-poly(2-phenyl-2-oxazoline), and poly(2-methyl-2-oxazoline)-*block*-poly(2-butyl-2-oxazoline). The hydrophilic ratio and molecular weights were varied in order to obtain a range of possible behaviors. Their self-assembly after nanoprecipitation or film rehydration was examined. The resulting nano-objects were fully characterized by transmission electron microscopy (TEM), cryo-TEM, multiple-angle dynamic and static light scattering, and X-ray scattering. In most cases, the formation of polymer micelles was observed, as well as, in some cases, aggregates, which made characterization more difficult. Crosslinking was performed under UV illumination in the presence of a coumarin-bearing crosslinker based on polymethacrylate derivatives. Addition of the photocrosslinker and crosslinking resulted in better-defined objects with improved stability in most cases.

INTRODUCTION

The field of nanomedicine involving the use of nanovectors to deliver biologically-relevant molecules in a controlled manner has revealed the importance of providing a wide variety of chemical structures for the vectors. Indeed, the target specifications for a specific application differ so much from one another that obviously no single vector could meet them all. In order to protect the target molecule and carry it to the desired location, vectors must exhibit adequate properties, firstly, for their outer part interacting directly with the biological medium, and, secondly, for their inner part interacting with the transported molecule. Therefore, a delicate equilibrium must be found in order to encapsulate the active molecule effectively, protect it during transport, and release it upon arrival at the delivery site. While poly(ethylene oxide) (PEO) is the most widely used hydrophilic part among these vectors (owing to its stealth property versus opsonization), there have been some cases of allergic reactions in patients, and some studies have reported that the stealth of PEO, while present upon the first injection, may be lost for subsequent ones.[1-4] The development of possible substitution solutions is therefore still needed. Polyoxazolines are one of the most promising leads, which have been examined for some years now in the field of biomaterial hydrogels[5-7] or drug delivery.[7-8] Polyoxazolines offer the enormous advantage of tunable chemistry. Indeed, they are obtained by cationic ring-opening polymerization of 2-alkyl-2-oxazolines, in a controlled process. This enables the synthesis of various polymer morphologies, from hydrophilic or hydrophobic homopolymers, to amphiphilic di- or triblock copolymers.[9-11] They also offer the option of introducing chemical functions along the polymer chain, such as alkenyl groups[12] or fluorinated moieties.[13-14] Once formed, the polyoxazoline (POXA) chain can furthermore be hydrolyzed into polyethyleneimine (PEI), providing access to additional

structures.[15-16] Recently, Schubert and coll. showed that this was also a way to transform the POXA chain into a degradable system by developing an oxidized PEI from POXA.[17]

The formation of nanovectors based on POXA usually involves poly(2-methyl-2-oxazoline) PMOXA or poly(2-ethyl-2-oxazoline) PEtOXA as hydrophilic blocks and other alkyl POXA as the hydrophobic part, such as 2-phenyl-2-oxazoline[18] or linear alkyl chains.[9, 13-14, 19] Interestingly, Luxenhofer and coll. recently showed that choosing between PMOXA or PEtOXA as the hydrophilic block had an effect on the loading capacity of the vector for two examples, namely curcumin and paclitaxel. This change in the loading capacity due to the external hydrophilic block for hydrophobic drugs was unexpected.[20]

In the field of nanovector formulation, it has been demonstrated several times that crosslinking the vector improved delivery, especially on 3D-cell culture.[21-23] However, only rare cases of crosslinked POXA systems have been described so far and most were aimed at forming gels[12, 16, 24] and not nano-objects.[25] Schubert and coll. used a light-assisted thiol-ene reaction to crosslink PMOXA-PdecenylOXA nano-objects[14], and studied their behavior in oil/water emulsions. Our group developed a different strategy based on coumarin-functionalized POXA.[26-27] We demonstrated that PMOXA, even with a very short hydrophobic part, results in the formation of objects. Furthermore, the addition of a coumarin-bearing crosslinker agent led to systems that could be used for photodynamic therapy.

In this study, we have widened the range of purely POXA amphiphilic block copolymers based on 2-methyl-2-oxazoline for the hydrophilic block and 2-phenyl and 2-butyl-2-oxazolines for the hydrophobic one. Here we present the synthesis together with the formation and characterization of self-assemblies as well as their photo-crosslinking in the presence of a

coumarin-bearing methacrylate copolymer PEHMA-co-CoumMA. This will provide new tools for future studies linked with nanomedicine as photoreactive nanovectors.

MATERIALS AND METHODS

4-Methylumbelliferone, 7-hydroxy-4-methylcoumarin, 11-bromoundecanol, diethylether, ethanol, acetone, p-toluenesulfonyl chloride, piperidine, pyridine, methacryloyl chloride, 2,2'-azobis(2-methylpropionitrile) (AIBN) $MgSO_4$, potassium carbonate (K_2CO_3) and dodecanethiol (DDT) were purchased from Sigma Aldrich and used without further purification. 2-ethylhexyl methacrylate was purchased from Alfa Aesar. 2-Methyl-2-oxazoline (MOXA), 2-phenyl-2-oxazoline (PhOXA), 2-*n*-butyl-2-oxazoline (BuOXA) and acetonitrile were distilled over CaH_2 just prior to use. Methacryloyl chloride was distilled under reduced pressure before use. Coumarin tosylate (CoumOTs) was synthesized and purified by recrystallization according to previously published protocols[26]. Acetonitrile and chloroform were distilled over CaH_2 and stored in nitrogen. All other commercial reagents and solvents were used as received. Ultrapure water was obtained from an ELGA Purelab Flex system (resistivity greater than 18.2 MΩ.cm) and was filtered on 0.2 μm RC filters just before use. ^1H and ^{13}C NMR Spectra were recorded using a Bruker Avance 300 MHz spectrometer.

Synthesis of Amphiphilic Diblock Copolymers CoumPhOXA$_m$-MOXA$_n$ and CoumBuOXA$_m$-MOXA$_n$. Amphiphilic diblock copolymers with various PhOXA, BuOXA and MOXA block lengths were successfully synthesized using the same procedure. Herein, CoumPh$_{31}$-MOXA$_{65}$ is described. All polymerizations were performed in a microwave oven (850 W). In a 30 mL vial equipped with a magnetic stirring bar, CoumOTs (0.253 g, 0.5 mmol, 1 eq) was dissolved in anhydrous acetonitrile (6 mL) in an N_2 atmosphere. 2-Phenyl-2-oxazoline (2.24 g, 15.16 mmol,

30 eq) was added. The vial was introduced into the micro-wave oven for 60 min at 140 °C. When the polymerization of the first block was achieved, the vial was removed from the oven, and 2-methyl-2-oxazoline (2.98 g, 35 mmol, 70 eq) was added to form the second block under the same conditions (140 °C for 60 min). The reaction was then quenched with piperidine (0.065 g, 0.75 mmol, 1.5 eq), and maintained at room temperature for 12 h under stirring. The reaction mixture was precipitated in cold diethyl ether, and the polymer was dried in a vacuum oven at 60 °C for 12 h.

CoumPhOXA$_m$-MOXA$_n$ (Figures S1-S5)

^{1}H NMR Spectroscopy (400 MHz, CDCl$_3$) δ (ppm): = 7.5-6.9 (m, H$_{c,3}$), 6.85 (s, 1H, H$_4$), 6.8 (s, H$_5$), 6.1 (s, H$_1$), 4 (m, H$_6$), 3.7-3 (m, H$_{a,\ b,16}$), 2.4 (s, H$_2$), 2.2-1.9 (m, H$_d$), 1.8-1.2 (m, H$_{7\text{-}15}$). The number of MOXA hydrophilic block repeat units (n) was calculated by integrating aromatic coumarin protons at 6.85 ppm associated with the peak at 2.1 ppm corresponding to CH$_3$-C=O of MOXA while the number of PhOXA hydrophobic block repeat units (m) was determined by integrating aromatic PhOXA protons at 7.3 ppm associated with 6.85 ppm.

^{13}C NMR (400 MHz, CDCl$_3$) δ (ppm): 172.1-170.8 (C$_{24,33}$), 162.2 (C$_4$), 161.2 (C$_7$), 149 (C$_2$), 148.1 (C$_5$), 135.57 (C$_{28}$), 129.6-126.3 (C$_{25,26,27,29,30,9}$), 112.9-109 (C$_{8,3,10}$), 101.2 (C$_6$), 68.3 (C$_{11}$), 67.1 (C$_{21}$), 47.5-40.9 (C$_{22,23,31,32}$), 30.5-15.6 (C$_{1,12,13,14,15,16,17,18,19,20,34}$).

CoumBuOXA$_m$-MOXA$_n$ (Figure S6)

^{1}H NMR Spectroscopy (400 MHz, CDCl$_3$) δ (ppm): = 7.5 (s, H$_3$), 6.85 (s, 1H, H$_4$), 6.8 (s, H$_5$), 6.1 (s, H$_1$), 4 (m, H$_6$), 3.7-3 (m, H$_{a,\ b,16}$), 2.4 (s, H$_2$), 2.2-2 (m, H$_d$), 1.9-1.2 (m, H$_{7\text{-}15,c,d,e}$), 0.9 (m, H$_f$). The number of BuOXA repeat units (m) was determined by comparing the coumarin signal to the CH$_3$- of BuOXA at 0.9 ppm.

^{13}C NMR Spectroscopy (400 MHz, $CDCl_3$) δ (ppm): 171.4-170.8 ($C_{31,32}$), 162.2 (C_4), 161.2 (C_7), 142.3 (C_2), 140.1 (C_5), 137.5 (C_9), 113.3-111.7 ($C_{8,3,10}$), 101.9 (C_6), 69.1 (C_{11}), 66,9 (C_{21}), 47.9-43.5 ($C_{22,23,29,30}$), 32.6-13.9 ($C_{1,12,13,14,15,16,17,18,19,20,24,25,26,27,28,32}$).

Synthesis of PEHMA-co-CoumMA 50/50 (X50-50, Figure S8). In a two-necked round-bottomed flask, CoumMA[28] (12.0 g, 28.9 mmol, 7.8 eq) was dissolved in 70 mL of butanone. 2-Ethylhexyl methacrylate (5.74 g, 28.9 mmol, 7.8 eq), 1-dodecanethiol (0.748 g, 3.7 mmol, 1 eq) and AIBN (95 mg, 0.58 mmol, 0.16 eq) were then added. The mixture was deoxygenated by circulating an argon flow for 10 min at room temperature, then heated at 70 °C overnight to perform the polymerization. When the maximum conversion rate was reached (96%), the mixture was cooled down to room temperature. Then, the solvent was removed by vacuum evaporation, and the crude product was solubilized in 15 mL of dichloromethane. The polymer was precipitated in 1 L of a 95/5 v/v Et_2O/Pentane mixture, then allowed to settle before removing the supernatant solvent. The product was dissolved again in dichloromethane, then concentrated in a vacuum until no solvent remained. PEHMA-co-CoumMA was obtained as a yellow viscous oil. The yield was 69% (12.8 g).

^{1}H NMR Spectroscopy (300 MHz, $CDCl_3$) δ (ppm): 7.40 (d, H_a), 6.75 (m, H_b), 6.04 (s, H_c), 3.95-3.64 (m, H_d), 2.38 (m, H_e), 2.32 (s, H_f), 2.00-0.70 (m, -CH_2 and -CH_3 aliphatic).

^{13}C NMR Spectroscopy (300 MHz, $CDCl_3$) δ (ppm): 177.56 (C_a), 162.20 (C_b), 161.24 (C_c), 155.27 (C_d), 152.55 (C_e), 125.46 (C_f), 113.37- 111.77 (C_g), 101.29 (C_h), 68.59 (C_i), 44.79 (C_j), 38.48 (C_k), 30.49-25.16 ($C_{aliphatic\ chains}$), 18.63 (C_l), 14.13 (C_m), 11.01 (C_n).

Synthesis of PEHMA-co-CoumMA 20/80 (X20-80, Figure S9). In a two-necked round-bottomed flask, CoumMA (16.0 g, 38.6 mmol, 10.3 eq) was dissolved in 70 mL of butanone. 2-

Ethylhexyl methacrylate (1.91 g, 9.63 mmol, 2.6 eq), 1-dodecanethiol (0.756 g, 3.74 mmol, 1 eq) and AIBN (79 mg, 0.48 mmol, 0.13 eq) were then added. The mixture was deoxygenated by circulating an argon flow for 10 min at room temperature, then heated at 70 °C overnight to perform the polymerization. When the maximum conversion rate was reached (91%), the mixture was cooled down to room temperate. Then, the solvent was removed by vacuum evaporation, and the crude product was solubilized in 15 mL of dichloromethane. The polymer was precipitated in 800 mL of a 95/5 v/v Et_2O/Pentane mixture, then allowed to settle before removing the supernatant solvent. The product was dissolved again in dichloromethane then concentrated in a vacuum until no solvent remained. PEHMA-co-CoumMA was obtained as a yellow solid. Yield: 78% (14.5 g).

^{1}H NMR Spectroscopy (300 MHz, $CDCl_3$) δ (ppm): 7.40 (d, H_a), 6.75 (m, H_b) , 6.04 (s, H_c), 3.95-3.64 (m, H_d), 2.38 (m, H_e), 2.32 (s, H_f), 2.00-0.70 (m, -CH_2 and -CH_3 aliphatic).

^{13}C NMR Spectroscopy (300 MHz, $CDCl_3$) δ (ppm): 177.56 (C_a), 162.20 (C_b), 161.24 (C_c), 155.27 (C_d), 152.55 (C_e), 125.46 (C_f), 113.37- 111.77 (C_g), 101.29 (C_h), 68.59 (C_i), 44.79 (C_j), 38.48 (C_k), 30.49-25.16 ($C_{aliphatic\ chains}$), 18.63 (C_l), 14.13 (C_m), 11.06 (C_n).

Formation of Polymer Self-assemblies by Nanoprecipitation. 10 mg of polymer and the desired amount of crosslinker (calculated as 1/1 mol/mol of coumarin units between POXA and the crosslinker) were dissolved in 0.4 mL of the chosen organic solvent (the final choices were iPrOH, except for CoumPhOXA$_{31}$-MOXA$_{65}$ / X20-80, for which DMF was used instead). The solution was dropped under magnetic stirring into 4 mL of water in ca. 5 min. The solution was stirred for 30 min. The removal of organic solvent was obtained either by evaporation by leaving the solution to stand for 2 days under a ventilating hood or by dialysis during 5 days (RC membrane with a 1 kDa MWCO).

Formation of Polymer Self-assemblies by Film Rehydration. 10 mg of polymer and the desired amount of crosslinker (calculated as 1/1 mol/mol of coumarin units between POXA and the crosslinker) were dissolved in 0.4 mL of chloroform. The solvent was then removed on a rotary evaporator for 1 h. The polymer film formed was dried further in a vacuum at room temperature overnight. 4 mL of filtered water was then added, and the suspension was heated at 65 °C for 30 min, followed by ultrasonication at 65 °C for 1 h.

Coumarin Dimerization. A 5-mm glass tube containing 2.2 mL of the self-assembly solution was placed at 8 mm between two UV lamps for 12 h (**Figure S10**), Philips linear T5 8W, irradiation at 360 nm, lamp-tube distance 8 mm, total irradiance 1.0 $mW.cm^{-2}$, measured with an HD9021 photometer from Delta Ohm Inc.

Characterization of the Critical Aggregation Concentration by Fluorimetry. The critical aggregation concentration (CAC) was determined by fluorimetry using an LS45 spectrometer (Shimatzu). Aggregate formation was examined over a wide range of polymer concentrations (1×10^{-3} - 0.2 $mg.mL^{-1}$) using pyrene as a fluorescent probe. Polymers were dissolved in Milli-Q water before filtration through 0.45 μm PTFE microfilters. The solutions were then diluted to the required concentration. 0.25 mL of a pyrene solution (1.9×10^{-3} M in methanol) was added to 24.75 mL of Milli-Q water. 75 μL of the pyrene solution was then added to the different polymer solutions (1.5 mL), leading to a final pyrene concentration of 9×10^{-7} M. The samples were excited at 340 nm and the emission spectra were recorded from 350 to 450 nm.[29-30] The average fluorescence values at the vibronic bands 384 nm (I_1) and 373 nm (I_3) were used for subsequent calculations. The CAC, determined by plotting the 373/384 (I_1/I_3) ratio *versus* the polymer

concentration was taken as the intersection of regression lines calculated from the linear portions of the graph.

Size-Exclusion Chromatography (SEC). POXA block copolymers were analyzed with a Varian 390-LC model equipped with a refractometric detector (880 nm). Two PL-gel mix C columns were used at 70 °C using *N*,*N*-dimethylformamide (DMF) (0.1 wt% LiBr) as an eluent, at a flow rate of 0.8 $mL.min^{-1}$. A poly(methyl methacrylate) (PMMA) calibration was used to determine the average molar weights using PMMA standards from Agilent. Samples were injected at a 10 $mg.mL^{-1}$ concentration. Methacrylic copolymers were analyzed with a Varian PL-GPC-50 Plus model equipped with a refractometric detector. Two Polypore columns were used at 35°C using tetrahydrofuran (THF) as an eluent, at a flow rate of 1 $mL.min^{-1}$. A PMMA (Poly(methyl methacrylate)) calibration was used to determine the average molar weights using PMMA standards from Agilent.

Differential Scanning Calorimetry (DSC). DSC thermograms were recorded using a Q2000 (TA Instruments) apparatus in a sealed pan under nitrogen flow (50 $mL.min^{-1}$). An empty pan was used as reference. Samples were analyzed from -80°C to 200°C with 10 $°C.min^{-1}$ heating and 10 $°C.min^{-1}$ cooling between the first and second run (the second heating run was used to calculate T_g).

Dynamic Light Scattering (DLS). DLS analyses were carried out at 25 °C on a Malvern (Orsay, France) Zetasizer NanoZS. The solutions were analyzed in triplicate without being filtered in order to characterize the plain samples. Data were analyzed using the general-purpose non-negative least squares (NNLS) method. The typical accuracy for these measurements was 10-20% for systems exhibiting a polydispersity index of less than 0.4. To provide a full image of the

dispersity of the results obtained between batches, intensity- and number-average results are provided for 4 different sets of film rehydration: CoumPhOXA$_{31}$-MOXA$_{65}$ alone, with X20-80 crosslinker but non-crosslinked, with X20-80 crosslinker and crosslinked, and CoumPhOXA$_{64}$-MOXA$_{104}$ (**Figure S11**). Number-average values were found to be very reproducible between batches. In some instances, intensity-average values exhibited larger values (**Figure S11)**. In some cases, multiangle dynamic light scattering was performed with an LS Spectrometer (LSinstruments) in 3D configuration measuring scattering from 20 to 150° each 2 or 5°.

All correlograms were analyzed by a custom-made program named STORMS in order to obtain a more precise characterization of the solutions.[31] This program was designed with Matlab, and makes it possible to fit DLS correlograms using different sets of parameters, corresponding to all hypotheses to be made during treatment. Indeed, the transition from correlograms to size results implies three levels of hypotheses: the first consists in the transformation of autocorrelation data to a diffusion coefficient, the second one involves extracting the size of the scattering object from the diffusion coefficient based on its geometry, and, finally, a model is used enabling the transformation of the intensity-relative population to a number-relative one. For each step, STORMS provides a choice of different parameters. For the nano-objects described here, the protocol used NNLS fitting, assuming a spherical shape for all objects, and the chosen scattering model corresponded to a mixture of micelles and vesicles (maximum micelle size set to a radius of 25 nm). Different sets in respect of the range of decay rates and the regularization parameter were used, $\alpha = 5$ and range = 1 being the most appropriate values for the samples from this study. Unless stated otherwise, this treatment provided residuals of less than 5×10^{-3} for all analyses. The polydispersity index (PDI) is the ratio between the variance of the distribution and the square of the mean value of the decay rate, $\overline{\Gamma}$. When the autocorrelation functions were recorded at different

angles, $\overline{\Gamma}$ was plotted as a function of q^2 in order to retrieve the mean diffusion coefficient and, using the Stokes-Einstein equation, the mean hydrodynamic radius according to equation $\overline{\Gamma} = Dq^2$.

For the evaluation of DMF resistance, similar DLS experiments were performed by increasing the amount of DMF. The position of the measurements was fixed and the refractive index was changed according to the amount of DMF.

Transmission Electron Microscopy (TEM) and Cryo-TEM. Negatively stained specimens were prepared by first depositing droplets of dilute aqueous particle suspensions onto freshly glow-discharged copper grids supporting a carbon film. After 1-3 min, the excess liquid was absorbed with filter paper and, before complete drying, a droplet of 2 wt% uranyl acetate aqueous solution was deposited. The excess stain was blotted, and the preparations were allowed to air-dry. The specimens were observed with a Hitachi HT7700 microscope operating at an accelerating voltage of 80 kV and equipped with an AMT CCD camera, or a JEOL JEM-2100 Plus microscope operating at 200 kV and equipped with a Gatan Rio16 camera.

Cryo-TEM specimens were prepared by depositing a droplet of particle suspension onto glow-discharged Pelco NetMesh lacey carbon grids, then placed in the chamber of a Leica EM-GP automatic plunge freezer set at 20 °C and 95% relative humidity. The excess liquid was blotted and the grids were flash-frozen in liquid ethane (-185 °C). The frozen specimens were placed in a Gatan Elsa cryo-holder cooled with liquid nitrogen, and observed at a low temperature with the JEOL JEM-2100 Plus microscope, at 200 kV, under low-dose illumination. Images were recorded using the SerialEM software.[32]

Size distribution histograms were determined by measuring the diameter of populations of about 200 particles from the TEM images, using ImageJ software. The results were expressed as

mean diameters and standard deviations. In the presence of several populations, the distribution was deconvoluted using Gaussian functions with Origin or Prism software.

RESULTS AND DISCUSSION

As depicted in **Scheme 1**, the polymeric nanoparticles investigated in this study result from photo-crosslinking between amphiphilic block copolymers of coumarin-unit-terminated poly(2-alkyl-2-oxazoline) and a copolymer of ethylhexyl methacrylate and coumarin-bearing methacrylate (X50-50 or X20-80) used as a photocrosslinker. Because the synthesized polyoxazolines exhibited a single coumarin unit per chain, it was necessary to use a photocrosslinker with several coumarin units to ensure a real crosslinking of the self-assemblies. A polymer crosslinker was preferred, since it provided a simple manner to tune the affinity of the crosslinker to the polyoxazoline polymers, while facilitating a full coumarin dimerization. The influence of the nature of the hydrophobic block of the amphiphilic copolymer on self-assembly was studied using 2-butyl-2-oxazoline (CoumBuOXA-b-MOXA) and 2-phenyl-2-oxazoline (CoumPhOXA-b-MOXA). Please note that, in order to shorten the notation, the polymers will be named in the following manner : CoumAlkOXA$_n$-MOXA$_m$, Alk being either phenyl- or butyl-, n and m the respective degree of polymerization. Additionally, the influence of the hydrophobic/hydrophilic balance on self-assembly was investigated.

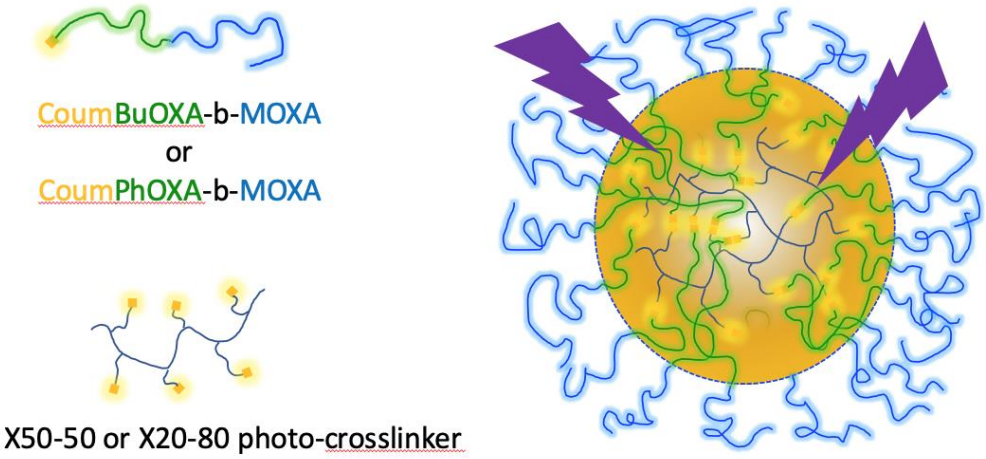

Scheme 1. General crosslinked polymer self-assembly formation strategy

Copolymer Synthesis. A range of amphiphilic block copolymers based on photosensitive coumarin, 2-phenyl or 2-butyl-2-oxazoline monomer (PhOXA and BuOXA) as a hydrophobic block, and 2-methyl-2-oxazoline monomer as a hydrophilic block were successfully synthesized. These amphiphilic copolymers were prepared by cationic ring opening polymerization (CROP) using a tosylate initiator CoumOTs bearing a photosensitive coumarin end-group with C_{11} aliphatic spacer as shown in **Scheme 2**. The CROP initiator CoumOTs was synthesized according to a previous study[26] and used to initiate the polymerization of either PhOXA or BuOXA monomers in order to obtain the first hydrophobic block, after 1 h at 140 °C in a microwave oven. The full conversion of the monomer was indicated by the disappearance in ^{1}H NMR of the protons of PhOXA or BuOXA monomers at 3.98 and 4.35 ppm, corresponding to the CH_2-CH_2-N backbone. Subsequently, this first block was used as a macro-initiator to form the second hydrophilic block MOXA by means of in-situ addition of the second monomer into the reaction mixture under the same experimental conditions (1 h at 140 °C in microwave oven). It is noteworthy that the opposite strategy consisting in synthesizing the hydrophilic block first then using it as a macroinitiator for

the synthesis of the hydrophobic block is not recommended. Indeed, the lower reactivity of the hydrophobic monomer causes incomplete consumption, and hence results in poor block definition. At the end, the reaction was quenched with piperidine to convert the oxazolinium end-group into a terminal amine. The composition and the molecular weight of the copolymers CoumPhOXA$_n$-MOXA$_m$ or CoumBuOXA$_n$-MOXA$_m$ determined by ^{1}H NMR spectroscopy are reported in **Table 1**.

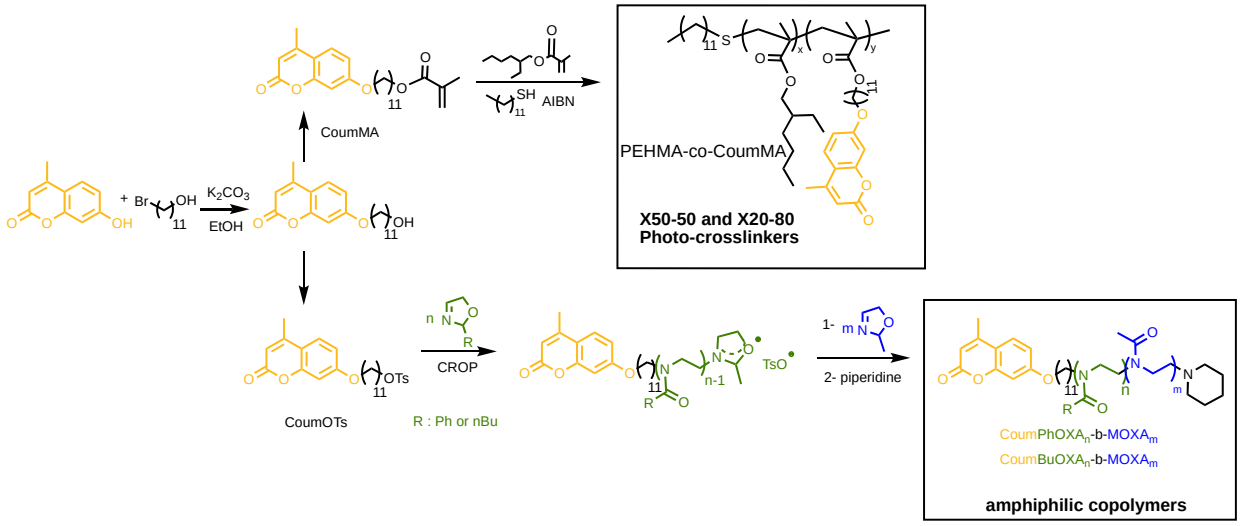

Scheme 2. Typical synthesis pathway for the copolymers

The SEC chromatograms shown in **Figure 1** are monomodal. The corresponding data are summarized in **Table S1**. In addition, two photo-crosslinkers of P(EHMA-co-CoumMA), X50-50 and X20-80 were synthesized by radical telomerisation using ethylhexyl methacrylate (EHMA) and a coumarin-bearing methacrylate (CoumMA) as comonomers in presence of AIBN (**Scheme 2)**. The compositions were calculated using ^{1}H NMR analysis: P(EHMA-co-CoumMA) 50/50, X50-50 (**Figure S8**) and PEHMA-co-CoumMA 20/80, X20-80 (**Figure S9**).

Table 1. Characteristics of amphiphilic copolymers.

Name	block 1	$M_{w,\ phobic}$ [a] (g.mol^{-1})	$M_{w,\ philic}$ [a] (g.mol^{-1})	$M_{w,\ total}$ [b] (g.mol^{-1})	Hydrophilic fraction

CoumPhOXA$_{31}$-MOXA$_{65}$	Phenyl	4600	5500	10400	0.53
CoumPhOXA$_{5}$-MOXA$_{68}$	Phenyl	740	5800	6900	0.85
CoumPhOXA$_{47}$-MOXA$_{33}$	Phenyl	6900	2800	10300	0.28
CoumPhOXA$_{64}$-MOXA$_{104}$	Phenyl	9400	8900	18600	0.48
CoumPhOXA$_{80}$-MOXA$_{65}$	Phenyl	11800	5500	17600	0.31
CoumBuOXA$_{9}$-MOXA$_{94}$	Butyl	1150	8000	9500	0.84

[a]: values based on ^{1}H NMR spectroscopy. [b]: $M_{w,\,total} = M_{w,\,phobic} + M_{w,\,philic} + M_{ext}$.

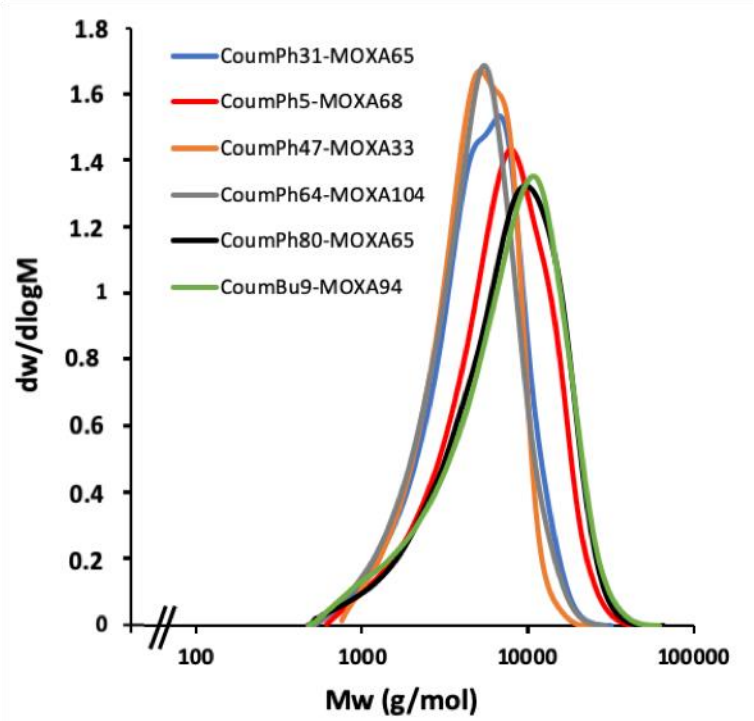

Figure 1. Superimposed SEC curves of the different POXA block copolymers.

Self-Assembly of Non-Crosslinked Systems. The ability of the polymers to form nano-objects is correlated with their critical aggregation concentration (cac). Several examples relating to poly(2-alkyl 2-oxazoline) copolymers have been described in the literature. For hydrophilic fractions between 0.5 and 0.7, the observed cac value has always been under 0.05 g.L^{-1}.[33-36] Only in extreme cases, such as a hydrophilic fraction of over 0.9, has the cac value been determined at

around 0.4 $g.L^{-1}$.[37] Based on these data, the cac value was measured only for $CoumPhOXA_{31}$-$MOXA_{65}$ by fluorimetry (**Figure S12**), and found to be around 0.02 $g.L^{-1}$, which was consistent with the literature. All subsequent experiments were thus performed at 2.5 $g.L^{-1}$, well above this threshold.

Different methods are routinely used for generating self-assembled nanovectors, namely nanoprecipitation, film rehydration, possibly combined with extrusion, or electroformation. The first part of this study consisted in evaluating the best conditions for forming reproducible nanovectors. The target specification for the method was a robust method with good reproducibility, with minimal toxic organic solvents, and uncontrolled precipitate formation. Electroformation was quickly ruled out owing to the low mobility of the polymer chains, linked with the glass transition temperatures above room temperature (**Table S1**). Therefore, we focused on nanoprecipitation and film rehydration. The principle of nanoprecipitation is based on using a good polymer solvent which should also be miscible with water. Due to the solubility of each polymer (**Table S2**), DMF or i-PrOH were more suitable, and resulted in well-formed objects exhibiting a TEM size of close to 20 nm. Given the high toxicity of DMF, i-PrOH was preferred, except in the case the X20-80 crosslinker, owing to its insolubility in iPrOH. The self-assemblies formed were characterized by dynamic light scattering (DLS) and transmission electron microscopy (TEM) (**Figure 2** and **Table 2**). $CoumPhOXA_{31}$-$MOXA_{65}$ was observed to form polymer micelles of around 20 nm. Combining with the crosslinkers led to a shift in size in DLS, especially for X50-50. This behavior was confirmed with TEM which revealed a marked deviation from Gaussian distribution. One hypothesis to explain this result is based on the lower compatibility of the X50-50 crosslinker with POXA polymers compared to the coumarin-rich X20-80 crosslinker.

Table 2. Characteristics of polymer self-assemblies formed by nanoprecipitation.

CoumPhOXA$_{31}$ -MOXA$_{65}$	Diameter DLS Int (nm)	Diameter DLS Num (nm)	PDI	Diameter TEM (nm)
alone	78	25	0.27	19 ± 4
with X50-50	241	144	0.22	35 ± 32
with X20-80	178	72	0.3	28 ± 7

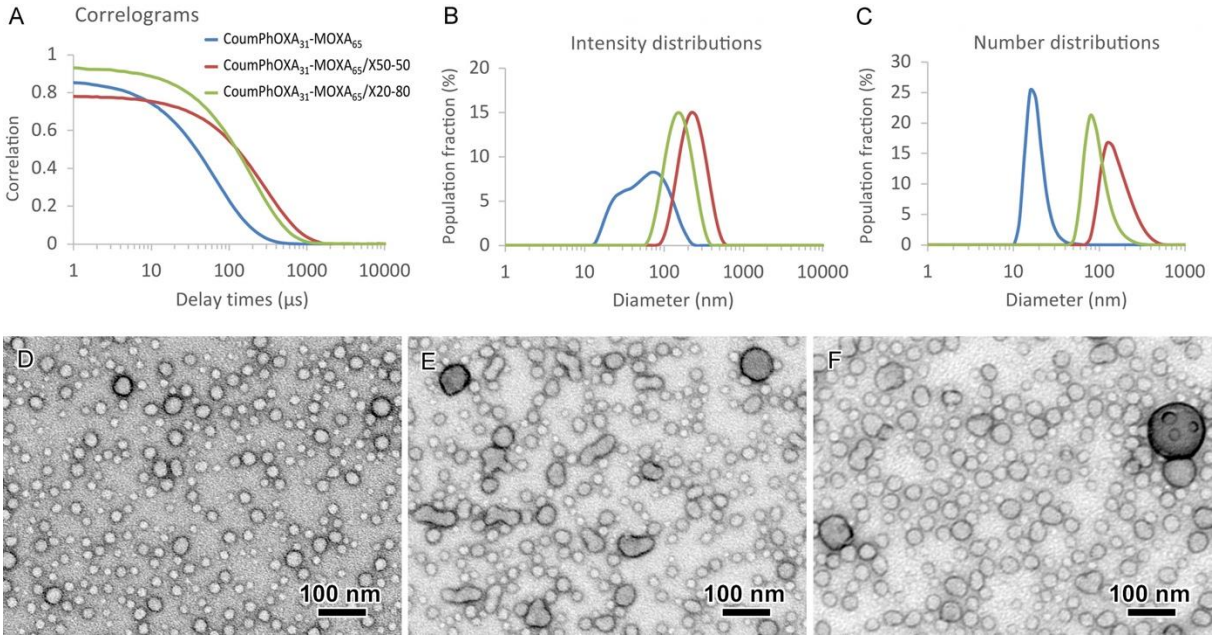

Figure 2. Characterizations of CoumPhOXA$_{31}$-MOXA$_{65}$ / X50-50 or X20-80 self-assemblies obtained by nanoprecipitation. DLS: A correlograms, B Intensity distribution, C Number distribution; TEM images of negatively stained preparations: D CoumPhOXA$_{31}$-MOXA$_{65}$, E CoumPhOXA$_{31}$-MOXA$_{65}$/X50-50, F CoumPhOXA$_{31}$-MOXA$_{65}$/X20-80. The size distributions from TEM images are shown in **Figure S13**.

The impact of film rehydration was then assessed using CoumPhOXA$_{31}$-MOXA$_{65}$. Chloroform was selected to form the dry film, as it solubilized both the POXA polymers and the crosslinkers. To form homogeneous polymer self-assemblies using the film rehydration method, extrusion is usually used. In our case, we observed using DLS and TEM that regular objects were already obtained with simple film rehydration and sonication. Extrusion did not improve the

distribution of the object formed (**Figure S14)**. Therefore, no extrusion was performed in the subsequent experiments.

All polymer self-assemblies were characterized using DLS and TEM (**Table 3**). The example of CoumPhOXA$_{31}$-MOXA$_{65}$ is shown in **Figures 3 and S15**. In the presence of X50-50, a minor population of objects exhibiting a size larger than 100 nm was very often observed, along with a major population between 15 and 40 nm (**Tables 3** and **S3**). In order to better visualize the distributions, cryo-TEM was also performed in some cases. In the case of CoumPhOXA$_{31}$-MOXA$_{65}$ / X50-50, TEM and cryo-TEM showed that the small objects represented the major population. Use of the X20-80 crosslinker, richer in coumarin units, did not show a strong tendency to yield large aggregates. Furthermore, the colloidal stability over time of the solutions was much improved in the presence of this crosslinker compared to X50-50. Therefore, all subsequent experiments were performed with the X20-80 crosslinker only. The copolymers with a hydrophilic fraction close to 0.5 resulted in the formation of well-formed micelles, and the size did not significantly increase upon incorporating the X20-80 crosslinker (**Table 3** and **Figure S16**). For the polymers with a hydrophilic fraction around 0.3, the formation of solid particles was observed, as revealed by cryo-TEM for CoumPhOXA$_{80}$-MOXA$_{65}$ (**Figure S16**). This result is surprising since many amphiphilic copolymers within this hydrophilic fraction range have been shown to form polymersomes.[38] The more hydrophilic polymers with a hydrophilic ratio above 0.8 resulted in possible mixtures of spheres and elongated particles. This is especially true for CoumBuOXA$_{9}$-MOXA$_{94}$ for which the presence of butyl groups presumably imparted a different hydrophobicity compared to phenyl groups and also a higher mobility of the chain itself, as indicated by a lower glass transition compared to the other copolymers (**Table S1** and **Figure S7**).

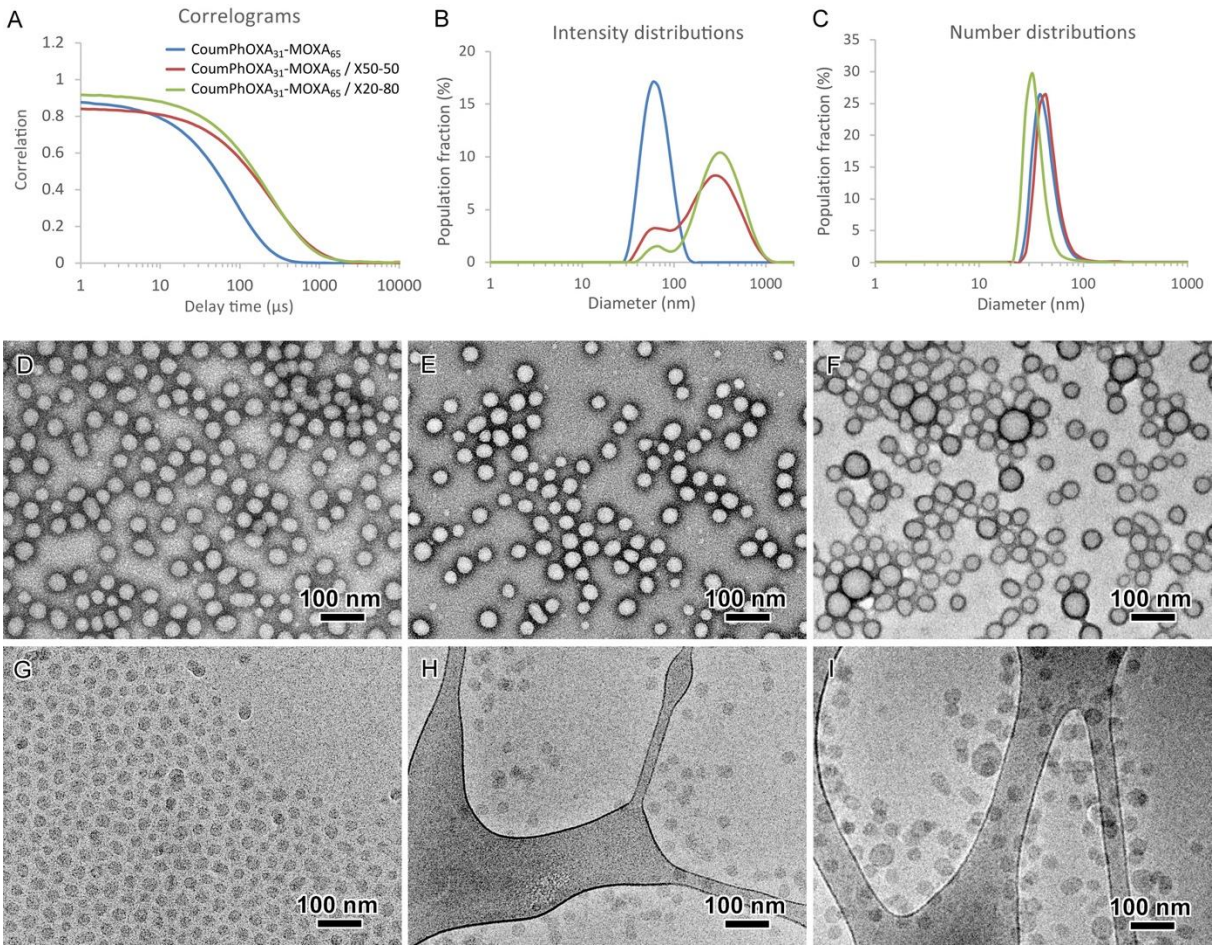

Figure 3. Characterization of CoumPhOXA$_{31}$-MOXA$_{65}$/X50-50 or X20-80 self-assemblies obtained with film rehydration and sonication. DLS: A) correlograms, B) intensity distributions, C) number distributions; TEM images of negatively stained preparations: D) CoumPhOXA$_{31}$-MOXA$_{65}$, E) CoumPhOXA$_{31}$-MOXA$_{65}$/X50-50, F) CoumPhOXA$_{31}$-MOXA$_{65}$/X20-80; cryo-TEM images: G) CoumPhOXA$_{31}$-MOXA$_{65}$, H) CoumPhOXA$_{31}$-MOXA$_{65}$/X50-50, I) CoumPhOXA$_{31}$-MOXA$_{65}$/X20-80. The size distributions from TEM and cryo-TEM images are provided in **Figures S15 and S16**.

Table 3. Characteristics of polymer self-assemblies formed by film rehydration.

Sample	f	DLS Int (nm)	DLS Num (nm)	PDI	MA[a] DLS (nm)	PDI MA DLS	Dg[b] MALS (nm)	Rg/Rh	TEM[c,d] (nm)	Cryo-TEM[c] (nm)
CoumPhOXA$_{31}$-MOXA$_{65}$	0.53	64	40	0.1	54	0.2	56±4	1.0	28 ± 6	28 ± 4
CoumPhOXA$_{31}$-MOXA$_{65}$/ X50-50		300/80	43	0.4	n.d.	n.d.	n.d.	n.d.	35 ± 6	30 ± 11
CoumPhOXA$_{31}$-MOXA$_{65}$/ X20-80		226/40	36	0.2	30/160	0.3	90±30[e]	-	41 ± 8	27 ± 10
X CoumPhOXA$_{31}$-MOXA$_{65}$/ X20-80		168/42	38	0.2	30/160	0.3	80±20[e]	-	34 ± 10	23 ± 5
CoumPhOXA$_{47}$-MOXA$_{33}$	0.28	29/110	25	0.1	30/300	>0.5	90±10[e]	-	25 ± 5	n.d.
CoumPhOXA$_{47}$-MOXA$_{33}$ / X20-80		160/26	24	0.3	194	0.2	218±10	1.1	27 ± 4	n.d.
X CoumPhOXA$_{47}$-MOXA$_{33}$ / X20-80		160/28	25	0.3	188	0.2	218±10	1.1	25 ± 10[f]	n.d.
CoumPhOXA$_{80}$-MOXA$_{65}$	0.31	100	86	0.1	134	0.3	110±10/260±40	1.0	84 ± 10 12 ± 6	48 ± 11
CoumPhOXA$_{80}$-MOXA$_{65}$ / X20-80		102	90	0.1	110	0.2	84±4	0.8	87 ± 13 15 ± 7	70 ± 14
X CoumPhOXA$_{80}$-MOXA$_{65}$ / X20-80		102	88	0.1	110	0.2	86±4	0.8	78 ± 13 21 ± 6	56 ± 12
CoumPhOXA$_{64}$-MOXA$_{104}$	0.48	69	47	0.1	62	0.2	62±4	1.0	38 ± 5	25 ± 5
CoumPhOXA$_{64}$-MOXA$_{104}$ / X20-80		75	49	0.1	68	0.2	66±4	1.0	51 ± 26[g]	25 ± 6
X CoumPhOXA$_{64}$-MOXA$_{104}$ / X20-80		76	49	0.1	68	0.2	72±6	1.1	29 ± 7	25 ± 6
CoumPhOXA$_{5}$-MOXA$_{68}$	0.85	13/58/510	9	0.6	30/300	>0.5	90±30[e]	-	58 ± 46[g]	n.d.
CoumPhOXA$_{5}$-MOXA$_{68}$ / X20-80		190	97	0.2	180	0.2	198±20	1.1	30±15	Too few objects
X CoumPhOXA$_{5}$-MOXA$_{68}$ / X20-80		194	96	0.2	180	0.2	190±20	1.1	38 ± 23[h]	44 ± 24[h]
CoumBuOXA$_{9}$-MOXA$_{94}$	0.84	100/410	15	1.0	20/200	>0.5	80±10 /220±20	-	some spheres & worm-like	n.d.
CoumBuOXA$_{9}$-MOXA$_{94}$ / X20-80		200/35	25	0.3	30/280	>0.5	98±10 / 350±20	-	some spheres & worm-like	n.d.

X CoumBuOXA$_9$-MOXA$_{94}$ / X20-80	44/530	18	0.4	36/320	>0.5	100±10/350±20	some spheres & worm-like	n.d.

[a] Multi-angle DLS measurements performed at angles ranging from 15° to 150°. [b] Diameter of gyration obtained with Guinier fit of the linear region of the plot ln(I(q)) vs q^2. [c] Mean values and standard deviation of the analysis of the population. [d] Negatively stained preparations. [e] Detection of poorly defined large aggregates. [f] Very small particles (< 5 nm) visible, not counted. [g] Presence of objects with various shapes, and possible aggregation. [h] Low number of particles, poorly resolved.

Self-Assembly of Crosslinked Systems. The self-assemblies formed were subsequently crosslinked under UV illumination (**Scheme 1**). Hereinafter, crosslinked systems will be differentiated from non-crosslinked ones by the prefix "X". The optimal reaction time was assessed by ^{1}H NMR in $CDCl_3$ after recovering the polymers from the irradiated solution by freeze-drying and re-suspending them in deuterated chloroform. A time of 12 h is required to reach 95 % dimerized coumarins (**Figure S17**). All self-assemblies formed in the first part were crosslinked using this procedure and characterized using the same techniques, namely single-angle DLS, TEM and cryo- TEM (**Table 3**). DLS and TEM showed that crosslinking did not result in any changes in the self-assemblies (**Figures 4** and **S18-23)**. TEM analyses were also performed one month after particle formation. The specimens showed no changes (data not shown), proving that both crosslinked and non-crosslinked vectors were stable for at least one month in pure water at room temperature. The crosslinking efficiency was also evaluated by exposing the particle solution to increasing amount of DMF, demonstrating a good resistance of crosslinked systems compared to non-crosslinked ones (**Figure S26**).

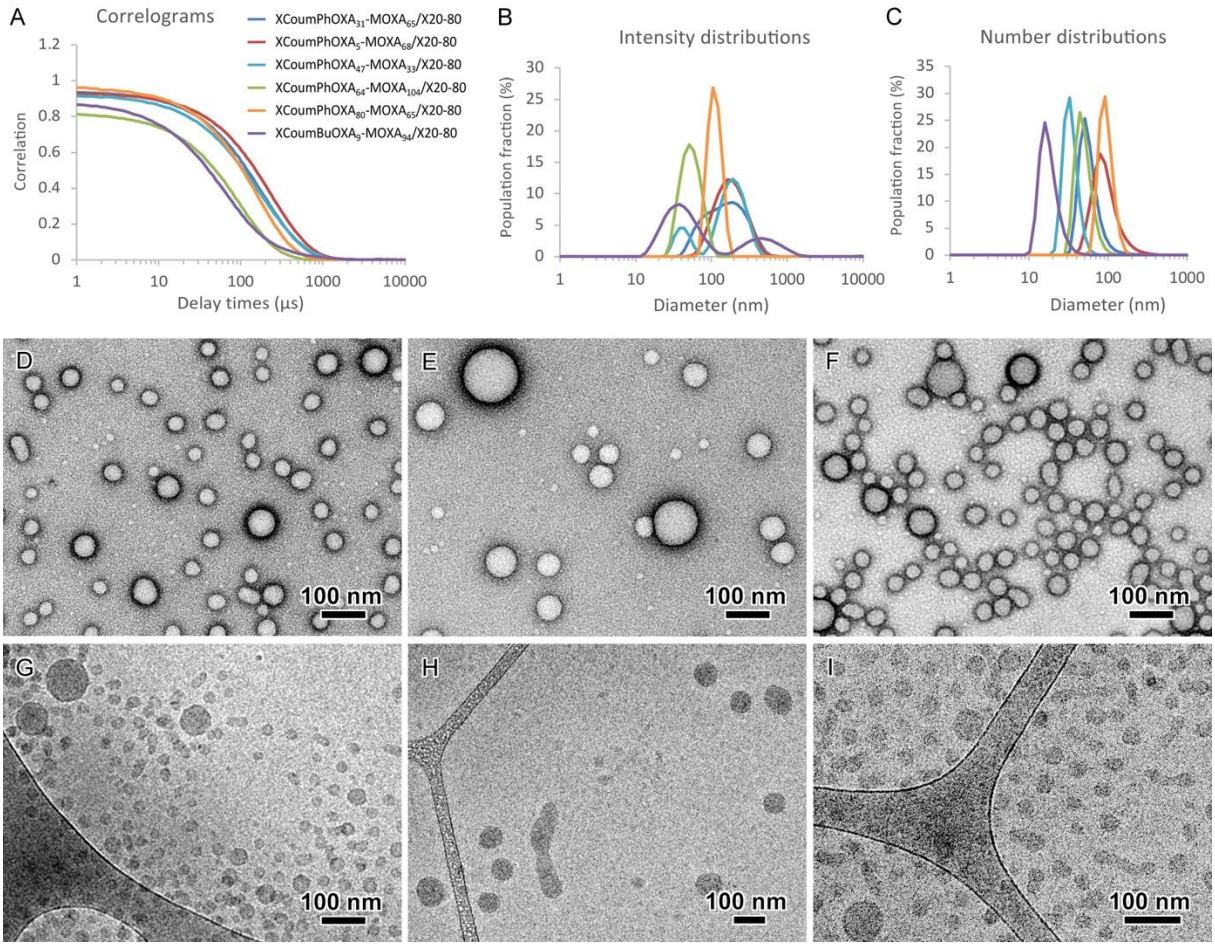

Figure 4. Characterization of crosslinked polyoxazolines / X20-80 self-assemblies obtained with film rehydration and sonication. DLS: A) correlograms; B) intensity distributions; C) number distributions; TEM images of negatively stained preparations: D) XCoumPhOXA$_{31}$-MOXA$_{65}$/X20-80; E) XCoumPhOXA$_{5}$-MOXA$_{68}$/X20-80; F) XCoumPhOXA$_{64}$-MOXA$_{104}$/X20-80; cryo-TEM images: G) XCoumPhOXA$_{31}$-MOXA$_{65}$/X20-80; H) XCoumPhOXA$_{5}$-MOXA$_{68}$/X20-80; I) XCoumPhOXA$_{64}$-MOXA$_{104}$/X20-80. The size distributions for TEM and cryo-TEM images are provided in **Figures S24 and S25**.

Multi-Angle Light Scattering Characterization. Because some self-assemblies contained several populations, the samples were further analyzed with multi-angle light scattering. SLS and DLS analyses at different angles ranging from 15 to 150° were performed on samples prepared by the rehydration method. The mean value of the hydrodynamic diameter together with the polydispersity index are reported in **Table 3**. The results are consistent with those obtained at 173°

in the case of less polydisperse samples. SLS curves are used to determine the radius of gyration (R_g) of the self-assemblies by fitting, where possible, the scattering curve to equation (1) (**Table 3**)

$$I(q) = I_0 \exp(-\frac{R_g^2}{3} q^2) \text{ or } \ln\big(I(q)\big) = ln(I_0) - \frac{R_g^2}{3} q^2 \qquad (1)$$

with a maximum q value $q_{max} \sim 1.3/R_g$. **Figure 5** shows the scattering curves normalized by the Rayleigh ratio of toluene in the case of samples containing the polymer only (**Figure 5a**) and the polymer in the presence of the cross-linking agent (X20-80) (**Figure 5b**).

*Poly(2-alkyl 2-oxazoline) Self-Assemblies (**Figure 5a**).* SLS measurements showed two very distinct level of intensities between the samples, the most hydrophilic ones exhibiting a very low level. An increase in the scattering intensity proportional to the molecular weight of the self-assembly can be observed. Furthermore, in some cases the presence of a power law trend for low scattering vectors is observed, which could be attributed to large self-assemblies or clusters (or aggregates) and makes the determination of the radius of gyration difficult in the absence of a clear Guinier region. In the case of CoumPhOXA$_5$-MOXA$_{68}$, CoumBu$_9$-MOXA$_{94}$ (hydrophilic fraction ~ 0.8) and CoumPhOXA$_{47}$-MOXA$_{33}$ (hydrophilic fraction ~ 0.3), a low *q* increase is always present independently of the preparation. Two linear regions are observed in the Guinier plot indicating the presence of two populations as also assessed with DLS. It is noteworthy that the PDI values of these samples are quite high (PDI > 0.5). For the other samples, the power law trend could be observed to different extents depending on some poorly identified experimental parameters (dry film characteristics, sonication power, etc.) and could reasonably be attributed to spurious aggregates.

The presence of these large nano-objects, even in small amounts, affects the results of the DLS measurements and explains the discrepancies with the TEM images. While the size of the self-

assemblies obtained with TEM is quite reproducible, the mean size obtained with scattering experiments (DLS or SLS) is strongly affected by the polydispersity of the samples.

Poly(2-alkyl 2-oxazoline)s/X20-80 Self-Assemblies. With the exception of CoumPhOXA$_{64}$-MOXA$_{104}$ and CoumPhOXA$_{80}$-MOXA$_{65}$ the addition of the cross-linking polymer induced an increase in the scattering intensity, but to different extents according to the polymer, depending on the hydrophilic ratio and the nature of the hydrophobic block. This is particularly striking in the case of CoumPhOXA$_{5}$-MOXA$_{68}$ (hydrophilic ratio ~0.8) where the scattering intensity increases by two orders of magnitude and reasonably monodisperse self-assemblies of about 90-100 nm radius are formed (**Figure 5b**). Interestingly, in the case of CoumBuOXA$_{9}$-MOXA$_{94}$, with a similar hydrophilic ratio, the increase in the scattering intensity is less marked, the size of the self-assemblies is increased only slightly, and aggregates are still present. In both cases, the copolymer alone was shown to yield only poorly defined self-assemblies linked to its high hydrophilicity. In the case of CoumPhOXA$_{5}$-MOXA$_{68}$, it can be assumed that the addition of hydrophobic X20-80 results in nanoparticles that are effectively stabilized by the copolymer. Due to the different nature of the hydrophobic block, the effect of the addition of the cross-linking agent is different in the case of CoumBuOXA$_{9}$-MOXA$_{94}$ even though it has the same hydrophilic ratio and the molecular weight of the two blocks is comparable.

The presence of aggregates is observed for several systems. This is the case for CoumPhOXA$_{31}$-MOXA$_{65}$/ X20-80 where, as for the polymer alone, some large assemblies (probably spurious aggregates) making it difficult to accurately determine the size using scattering techniques, are present. As seen in **Table 3**, the values have a high level of uncertainty; nevertheless, the minimum value is consistent with that evaluated with TEM, indicating that the size is only slightly influenced by the presence of the cross-linking agent. The case of

CoumPhOXA$_{64}$-MOXA$_{104}$ is more intriguing as no effect, neither in the scattering intensity nor in the size of the self-assemblies, is observed. CoumPhOXA$_{31}$-MOXA$_{65}$ and CoumPhOXA$_{64}$-MOXA$_{104}$ have the same hydrophilic ratio (~0.5), so this could be attributed either to the different molecular weight of the hydrophobic block or to differences in aggregates.

The scattering profile is also substantially modified in the case of CoumPhOXA$_{47}$-MOXA$_{33}$ (hydrophilic ratio 0.28), the scattering intensity increasing by one order of magnitude as well as the average size. For CoumPhOXA$_{80}$-MOXA$_{65}$, the addition of the cross-linking agent induces the formation of better defined, less polydisperse samples, comparable in size and scattering intensity to the initial ones. As in the case of the samples with a hydrophilic ratio ~0.5, the effect of X20-80 is more marked in the case of the copolymer with the smaller hydrophobic block.

For the lower hydrophilic ratios, the effect of the cross-linker seems to be linked with the molecular weight of the copolymer: the higher the molecular weight of the copolymer the smaller the effect on the size of the self-assemblies. On one hand, the scattering profile is substantially modified in the case of CoumPhOXA$_{47}$-MOXA$_{33}$ and CoumPhOXA$_{31}$-MOXA$_{65}$: the scattering intensity increases by about one order of magnitude and the overall size of the self-assemblies increases. On the other, CoumPhOXA$_{64}$-MOXA$_{104}$ and CoumPhOXA$_{80}$-MOXA$_{65}$ are not or only slightly influenced by the presence of the cross-linker, respectively. For CoumPhOXA$_{64}$-MOXA$_{104}$, no effect is observed, neither in the scattering intensity nor in the size of the self-assemblies. In the case of CoumPhOXA$_{80}$-MOXA$_{65}$ the addition of the cross-linking agent induces the formation of better defined, less polydisperse samples, comparable in size and scattering intensity to the initial ones.

Finally, characterization by DLS and SLS gives access to the R_g/R_h ratio (**Table 3**), providing information on the possible nano-object morphology. Most values were found close to 1, which would theoretically correspond to vesicles. However, TEM and cryo-TEM images do not reveal

the usual aspect for hollow objects and they preferably point to filled systems such as polymeric micelles or solid-like particles. A possible explanation is that, as already mentioned, the light scattering technique is extremely sensitive to the large aggregates and the present polydispersity therefore affects the R_g/R_h determination.

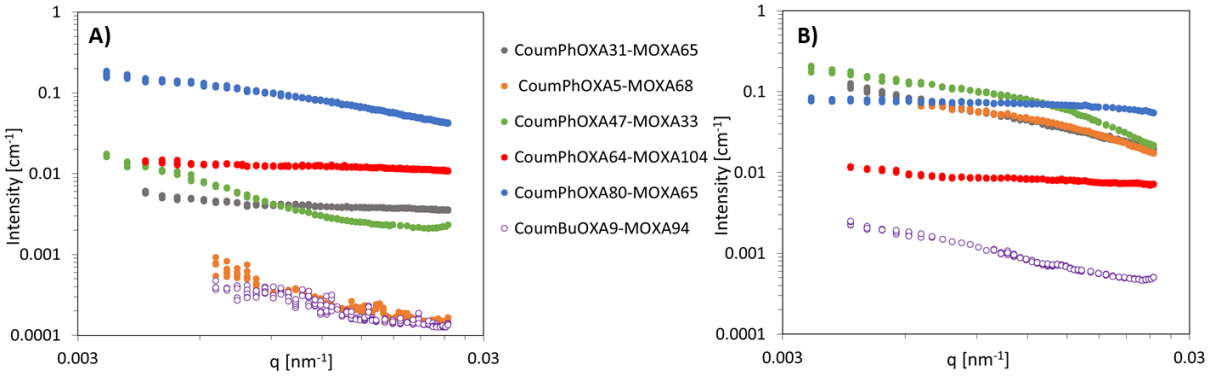

Figure 5. Multi-angle light scattering characterization of the self-assemblies without (A) and with (B) the X20-80 cross-linker

The overall analysis of these characterizations emphasized the crucial role of X20-80 as crosslinker. The changes were mainly brought by the addition of X20-80 to the polymer self-assemblies. The most noticeable modifications were observed for the most hydrophilic systems probably due to the stabilization action of the hydrophilic polyoxazoline on a hydrophobic X20-80 nanoparticle. For the lower hydrophilic ratios, the effect is mostly linked to the molecular weight of the hydrophobic block and the addition of few percentages of the crosslinker has few or no effect on the hydrophilic/hydrophobic balance for the higher molecular weight. It is furthermore noteworthy that no significant difference in size and morphology was noticed between not-crosslinked and crosslinked self-assemblies. Finally, as already mentioned, the crosslinking induced a higher stability of the self-assemblies to the addition of a good solvent.

Critical Comparison of the Different Techniques. Characterizing the nanovectors before their use is essential and must be performed with caution. Indeed, the behavior of the final drug delivery may vary if the composition, size distribution, and surface charge, etc., are not accurately known.[39-40] DLS and TEM are routinely used to characterize nanovectors.[41] Whereas both techniques are easily accessible to many groups, they both have advantages and drawbacks. DLS provides a hydrodynamic diameter from a measurement over a volume scanned by the laser, typically in the microliter range, reflecting the hydrodynamic size of the object in its end use. This value can be considered to be meaningful for describing the population of particles. However, while DLS is ideal for characterizing the size of perfectly similar and monodisperse particles, it quickly becomes inadequate for a population with a large size-distribution or multimodal solutions of mixtures of particles.[31] DLS alone cannot be relied upon to provide a size of the nano-objects. TEM is often used as a complementary technique and is very useful for revealing the presence of several populations that were not detected by DLS. However, it is well known that drying and/or staining the preparations may promote artefacts such as particle redistribution due to capillary forces, size-dependent preferential adsorption of the nanosystems on the carbon film, or deformation if the particles are soft or liquid-like. Furthermore, depending on the image magnification and field of view, TEM images often show a limited number of objects, which is not necessarily statistically relevant. It is therefore highly recommended to record several images of a given solution in different regions of the TEM grid. Basically, a minimum number of a few hundred objects should be considered as a representative dataset.

In our earlier research dealing with polyoxazoline-based nanovectors for photodynamic therapy,[27] we observed that these systems resulted in mixtures of populations and that their characterization was difficult. In this study, as we were anticipating similar behavior, we conducted a thorough assessment of nano-object size and morphologies combining different techniques.

Single-angle DLS was carried out as the first routine measurement, but was enhanced with data from multi-angle DLS and static light scattering (SLS) analyses. As already discussed, the results obtained from the multi-angle analysis corroborated those collected with routine mono-angle DLS. However, the presence of aggregates was detected more clearly, and an analysis without their influence was assessed. Moreover, the determination of the radius of gyration provided more information, giving indications on the morphology of the self-assemblies.

Similarly, while TEM was also performed systematically for all samples, cryo-TEM was performed on most (but not all) of them. In most cases, the aim was to evaluate possible artefacts due to drying and/or staining. The type of objects observed with both techniques was very often similar. The size determined from cryo-TEM images was generally smaller than that from TEM micrographs, which might be attributed to differences in contrast. Indeed, uranyl acetate was used as staining agent for dry preparations, whereas the cryo-TEM specimens were unstained. Negative staining is supposed to provide an imprint around the particle surface. With cryo-TEM, the shape and size of the particle, embedded in the film of vitreous ice, would be preserved. However, if the particles are formed of a dense core and a thin corona swollen in water, the contrast likely only reveals the electron-dense hydrophobic core. These effects would partly explain the difference in size between both techniques.

In addition, due to the inherent data processing, DLS provides several values, from the Z-average to the intensity- or number-averages, each case implying different hypotheses (shape, morphology, size range, etc…) and choices (CONTIN, NNLS, etc…). On the other hand, measuring the particle size from TEM images generally provides number-average values, to which a mathematical formula can be applied to calculate the equivalent of a Z-average mean size. Therefore, for the comparison of DLS and TEM average sizes to be meaningful, it is important to compare either the number-average or the Z-average mean values.

Finally, comparing our results to the literature confirms the original behavior of polyoxazoline copolymers. Indeed, for other types of amphiphilic block copolymers, a suggested rule of thumb is that vesicles are favored for hydrophilic fractions close to 0.3 and micelles for those close to 0.5.[42] In-between, worm-like systems have been observed. We have previously shown that a similar trend could be observed for poly(ethylene oxide)-*block*-poly(ε-caprolactone), although it was not possible to predict the morphologies based only on this parameter.[38] However, examining the self-assemblies based on polyoxazolines previously described shows that such a trend is barely present. Indeed, various morphologies have been described for low hydrophilic fractions below 0.4 (tubes, multicompartment vesicles, vesicles, worm-like systems)[19], but also for higher ratios around 0.6.[9, 18] Micelles have been obtained for a large range of hydrophilic ratios, from 0.4 to 0.7.[9, 18-20] In our study, we obtained objects with a filled core, as shown from the cryo-TEM images, most probably corresponding to micellar structures.

CONCLUSION

In the field of polymer nanovectors, a large number of systems have been assessed in the literature. As drug delivery outcomes and efficacy are strongly linked with the precise nature of the vectors, thorough characterization is essential before any biological evaluation. In this study, we have shown that poly(2-oxazoline) amphiphilic block copolymers were good candidates, due to their ability to self-assemble in water. Film rehydration without extrusion proved to be the most effective and reproducible method. The characterization of the resulting particles has proved to be difficult, owing to the presence of aggregates. However, by combining complementary techniques, we examined the particle size and morphology for each system. Among the different copolymers, those with a high hydrophilic ratio (> 0.8) formed very loose self-assemblies which were therefore not reliable candidates for nanovectorization. The other copolymers with hydrophilic ratios between

0.3 and 0.5 all resulted in polymeric micelles with sizes spanning from 25 to 90 nm. Co-encapsulation of a coumarin-bearing polymethacrylate was shown to result in better-defined self-assemblies in most cases. The effect is especially marked for the most hydrophilic systems. The potential of the less hydrophilic polymers as nanovectors of photosensitizers for photodynamic therapy will be described in a future publication.

ASSOCIATED CONTENT

Data on the synthesis and characterizations of all polymers. TEM and cryo-TEM images with particle size distribution analyses. Influence of the addition of DMF to the self-assemblies. The following files are available free of charge.

AUTHOR INFORMATION

Corresponding Authors

Anne-Françoise Mingotaud - *Laboratoire des IMRCP, Université de Toulouse, CNRS UMR 5623, Université Toulouse III - Paul Sabatier, 118 Rte de Narbonne, 31062 Toulouse cedex 9, France*. e-mail : anne-francoise.mingotaud@cnrs.fr

Vincent Lapinte - *ICGM, Université de Montpellier, CNRS, ENSCM, Montpellier, France.* e-mail : vincent.lapinte@umontpellier.fr

Authors

Kedafi Belkhir - *ICGM, Université de Montpellier, CNRS, ENSCM, Montpellier, France*

Orélia Cerlati - *Laboratoire des IMRCP, Université de Toulouse, CNRS UMR 5623, Université Toulouse III - Paul Sabatier, 118 Rte de Narbonne, 31062 Toulouse cedex 9, France*

Diana Heaugwane - *Laboratoire des IMRCP, Université de Toulouse, CNRS UMR 5623, Université Toulouse III - Paul Sabatier, 118 Rte de Narbonne, 31062 Toulouse cedex 9, France*

Alice Tosi - *Laboratoire des IMRCP, Université de Toulouse, CNRS UMR 5623, Université Toulouse III - Paul Sabatier, 118 Rte de Narbonne, 31062 Toulouse cedex 9, France*

Belkacem Tarek Benkhaled - *ICGM, Université de Montpellier, CNRS, ENSCM, Montpellier, France*

Pierre-Louis Brient - *Specific Polymers, 150 Avenue des Cocardières, 34160 Castries, France*

Camille Chatard - *Specific Polymers, 150 Avenue des Cocardières, 34160 Castries, France*

Alain Graillot - *Specific Polymers, 150 Avenue des Cocardières, 34160 Castries, France*

Sylvain Catrouillet - *ICGM, Université de Montpellier, CNRS, ENSCM, Montpellier, France*

Stéphanie Balor - *METi platform, Université Paul Sabatier, 118 route de Narbonne, 31062 Toulouse cedex, France*

Dominique Goudounèche - *CMEAB Université Toulouse III – Paul Sabatier, 133 Route de Narbonne 31062 Toulouse cedex, France*

Bruno Payré - *CMEAB Université Toulouse III – Paul Sabatier, 133 Route de Narbonne 31062 Toulouse cedex, France*

Pascale Laborie - *Technopolym, Institut de Chimie de Toulouse ICT-UAR 2599, Université Toulouse 3 – Paul Sabatier, 118 route de Narbonne, 31062 Toulouse cedex 9, France*

Jia-Hui Lim - *Univ. Grenoble Alpes, CNRS, CERMAV, F-38000 Grenoble, France*

Jean-Luc Putaux - *Univ. Grenoble Alpes, CNRS, CERMAV, F-38000 Grenoble, France*

Patricia Vicendo - *Laboratoire des IMRCP, Université de Toulouse, CNRS UMR 5623, Université Toulouse III - Paul Sabatier, 118 Rte de Narbonne, 31062 Toulouse cedex 9, France*

Laure Gibot - *Laboratoire des IMRCP, Université de Toulouse, CNRS UMR 5623, Université Toulouse III - Paul Sabatier, 118 Rte de Narbonne, 31062 Toulouse cedex 9, France*

Barbara Lonetti - *Laboratoire des IMRCP, Université de Toulouse, CNRS UMR 5623, Université Toulouse III - Paul Sabatier, 118 Rte de Narbonne, 31062 Toulouse cedex 9, France*

Author Contributions

The manuscript was written with contributions from all authors. All authors have approved the final version of the manuscript.

Funding Sources

This work was funded by the Occitanie Region and FEDER funds as the Pheophotodyn project.

ACKNOWLEDGMENTS

We would like to acknowledge the Occitanie Region and EU for their financial support (FEDER LR0021768: Pheophotodyn), as well as Yu Ogawa (CERMAV) for cryo-TEM observations and the NanoBio-ICMG Platform (UAR 2607) for granting access to the electron microscopy facility.

REFERENCES

1. Abu Lila, A. S.; Kiwada, H.; Ishida, T., The accelerated blood clearance (ABC) phenomenon: Clinical challenge and approaches to manage. *J. Controlled Release* **2013,** *172* (1), 38-47.
2. Knop, K.; Hoogenboom, R.; Fischer, D.; Schubert, U. S., Poly(ethylene glycol) in Drug Delivery: Pros and Cons as Well as Potential Alternatives. *Angewandte Chemie International Edition* **2010,** *49* (36), 6288-6308.

3. Schellekens, H.; Hennink, W. E.; Brinks, V., The Immunogenicity of Polyethylene Glycol: Facts and Fiction. *Pharm. Res.* **2013,** *30* (7), 1729-1734.
4. Yang, Q.; Lai, S. K., Anti-PEG immunity: emergence, characteristics, and unaddressed questions. *Wiley Interdisciplinary Reviews: Nanomedicine and Nanobiotechnology* **2015,** *7* (5), 655-677.
5. Wilson, P.; Ke, P. C.; Davis, T. P.; Kempe, K., Poly(2-oxazoline)-based micro- and nanoparticles: A review. *Eur. Polym. J.* **2017,** *88*, 486-515.
6. Dargaville, T. R.; Park, J.-R.; Hoogenboom, R., Poly(2-oxazoline) Hydrogels: State-of-the-Art and Emerging Applications. *Macromol. Biosci.* **2018,** *18* (6), 1800070.
7. Lorson, T.; Lübtow, M. M.; Wegener, E.; Haider, M. S.; Borova, S.; Nahm, D.; Jordan, R.; Sokolski-Papkov, M.; Kabanov, A. V.; Luxenhofer, R., Poly(2-oxazoline)s based biomaterials: A comprehensive and critical update. *Biomaterials* **2018,** *178*, 204-280.
8. Vlassi, E.; Papagiannopoulos, A.; Pispas, S., Amphiphilic poly(2-oxazoline) copolymers as self-assembled carriers for drug delivery applications. *Eur. Polym. J.* **2017,** *88*, 516-523.
9. Naka, K.; Nakamura, T.; Ohki, A.; Maeda, S., Aggregation behavior and interaction with human serum albumin of 2-oxazoline block copolymers in aqueous solutions. *Macrmol. Chem. Phys.* **1997,** *198* (1), 101-116.
10. Hoogenboom, R.; Wiesbrock, F.; Huang, H.; Leenen, M. A. M.; Thijs, H. M. L.; van Nispen, S. F. G. M.; van der Loop, M.; Fustin, C.-A.; Jonas, A. M.; Gohy, J.-F.; Schubert, U. S., Microwave-Assisted Cationic Ring-Opening Polymerization of 2-Oxazolines: A Powerful Method for the Synthesis of Amphiphilic Triblock Copolymers. *Macromolecules* **2006,** *39* (14), 4719-4725.
11. Monnery, B. D.; Hoogenboom, R., Thermoresponsive hydrogels formed by poly(2-oxazoline) triblock copolymers. *Polymer Chemistry* **2019,** *10* (25), 3480-3487.
12. Dargaville, T. R.; Lava, K.; Verbraeken, B.; Hoogenboom, R., Unexpected Switching of the Photogelation Chemistry When Cross-Linking Poly(2-oxazoline) Copolymers. *Macromolecules* **2016,** *49* (13), 4774-4783.
13. Kaberov, L. I.; Verbraeken, B.; Riabtseva, A.; Brus, J.; Radulescu, A.; Talmon, Y.; Stepanek, P.; Hoogenboom, R.; Filippov, S. K., Fluorophilic–Lipophilic–Hydrophilic Poly(2-oxazoline) Block Copolymers as MRI Contrast Agents: From Synthesis to Self-Assembly. *Macromolecules* **2018,** *51* (15), 6047-6056.
14. Rossegger, E.; Pirolt, F.; Hoeppener, S.; Schubert, U. S.; Glatter, O.; Wiesbrock, F., Crosslinkable/functionalizable poly(2-oxazoline)based micelles. *Eur. Polym. J.* **2019,** *121*, 109305.
15. Li, Y.; Vergaelen, M.; Pan, X.; Du Prez, F. E.; Hoogenboom, R.; De Clerck, K., In Situ Cross-Linked Nanofibers by Aqueous Electrospinning of Selenol-Functionalized Poly(2-oxazoline)s. *Macromolecules* **2018,** *51* (15), 6149-6156.
16. Li, Y.; Vergaelen, M.; Schoolaert, E.; Hoogenboom, R.; De Clerck, K., Effect of crosslinking stage on photocrosslinking of benzophenone functionalized poly(2-ethyl-2-oxazoline) nanofibers obtained by aqueous electrospinning. *Eur. Polym. J.* **2019,** *112*, 24-30.
17. Göppert, N. E.; Kleinsteuber, M.; Weber, C.; Schubert, U. S., Degradable Poly(2-oxazoline) Analogues from Partially Oxidized Poly(ethylene imine). *Macromolecules* **2020,** *53* (24), 10837-10846.
18. Krumm, C.; Fik, C. P.; Meuris, M.; Dropalla, G. J.; Geltenpoth, H.; Sickmann, A.; Tiller, J. C., Well-Defined Amphiphilic Poly(2-oxazoline) ABA-Triblock Copolymers and Their Aggregation Behavior in Aqueous Solution. *Macromol. Rapid Comm.* **2012,** *33* (19), 1677-1682.

19. Daubian, D.; Fillion, A.; Gaitzsch, J.; Meier, W., One-Pot Synthesis of an Amphiphilic ABC Triblock Copolymer PEO-b-PEHOx-b-PEtOz and Its Self-Assembly into Nanoscopic Asymmetric Polymersomes. *Macromolecules* **2020,** *53* (24), 11040-11050.
20. Haider, M. S.; Lübtow, M. M.; Endres, S.; Forster, S.; Flegler, V. J.; Böttcher, B.; Aseyev, V.; Pöppler, A.-C.; Luxenhofer, R., Think Beyond the Core: Impact of the Hydrophilic Corona on Drug Solubilization Using Polymer Micelles. *ACS Applied Materials & Interfaces* **2020,** *12* (22), 24531-24543.
21. Du, A. W.; Lu, H.; Stenzel, M. H., Core-Cross-Linking Accelerates Antitumor Activities of Paclitaxel–Conjugate Micelles to Prostate Multicellular Tumor Spheroids: A Comparison of 2D and 3D Models. *Biomacromolecules* **2015,** *16* (5), 1470-1479.
22. Lu, H.; Utama, R. H.; Kitiyotsawat, U.; Babiuch, K.; Jiang, Y.; Stenzel, M. H., Enhanced transcellular penetration and drug delivery by crosslinked polymeric micelles into pancreatic multicellular tumor spheroids. *Biomaterials Science* **2015,** *3*, 1085-1095.
23. Till, U.; Gibot, L.; Vicendo, P.; Rols, M. P.; Gaucher, G.; Violleau, F.; Mingotaud, A. F., Crosslinked Polymeric self-assemblies as an efficient strategy for photodynamic therapy on 3D cell culture. *RSC Advances* **2016,** *6*, 69984-69998.
24. Krumm, C.; Konieczny, S.; Dropalla, G. J.; Milbradt, M.; Tiller, J. C., Amphiphilic Polymer Conetworks Based on End Group Cross-Linked Poly(2-oxazoline) Homo- and Triblock Copolymers. *Macromolecules* **2013,** *46* (9), 3234-3245.
25. Brossier, T.; Benkhaled, B. T.; Colpaert, M.; Volpi, G.; Guillaume, O.; Blanquer, S.; Lapinte, V., Polyoxazoline hydrogels fabricated by stereolithography. *Biomaterials Science* **2022,** *10* (10), 2681-2691.
26. Korchia, L.; Bouilhac, C.; Lapinte, V.; Travelet, C.; Borsali, R.; Robin, J.-J., Photodimerization as an alternative to photocrosslinking of nanoparticles: proof of concept with amphiphilic linear polyoxazoline bearing coumarin unit. *Polymer Chemistry* **2015,** *6* (33), 6029-6039.
27. Oudin, A.; Chauvin, J.; Gibot, L.; Rols, M. P.; Balor, S.; Goudounèche, D.; Payré, B.; Lonetti, B.; Vicendo, P.; Mingotaud, A. F.; Lapinte, V., Amphiphilic polymers based on Polyoxazoline as relevant nanovectors for Photodynamic Therapy. *Journal of Materials Chemistry B* **2019,** *7*, 4973 – 4982
28. Korchia, L.; Lapinte, V.; Travelet, C.; Borsali, R.; Robin, J.-J.; Bouilhac, C., UV-responsive amphiphilic graft copolymers based on coumarin and polyoxazoline. *Soft Matter* **2017,** *13* (25), 4507-4519.
29. Aguiar, J.; Carpena, P.; Molina-Bolívar, J. A.; Carnero Ruiz, C., On the determination of the critical micelle concentration by the pyrene 1:3 ratio method. *J. Colloid Interface Sci.* **2003,** *258* (1), 116-122.
30. Guo, H.; Zhang, D.; Li, C.; Jia, L.; Liu, G.; Hao, L.; Zheng, D.; Shen, J.; Li, T.; Guo, Y.; Zhang, Q., Self-assembled nanoparticles based on galactosylated O-carboxymethyl chitosan-graft-stearic acid conjugates for delivery of doxorubicin. *International Journal of Pharmaceutics* **2013,** *458* (1), 31-38.
.31. Till, U.; Gibot, L.; Mingotaud, C.; Vicendo, P.; Rols, M. P.; Gaucher, M.; Violleau, F.; Mingotaud, A. F., Self-assembled polymeric vectors mixtures: characterization of the polymorphism and existence of synergetic effects in photodynamic therapy. *Nanotechnology* **2016,** *27*, 315102.
32. Mastronarde, D. N., SerialEM: A Program for Automated Tilt Series Acquisition on Tecnai Microscopes Using Prediction of Specimen Position. *Microscopy and Microanalysis* **2003,** *9* (S02), 1182-1183.

33. Babuka, D.; Kolouchova, K.; Loukotova, L.; Sedlacek, O.; Groborz, O.; Skarkova, A.; Zhigunov, A.; Pavlova, E.; Hoogenboom, R.; Hruby, M.; Stepanek, P., Self-Assembly, Drug Encapsulation, and Cellular Uptake of Block and Gradient Copolymers of 2-Methyl-2-oxazine and 2-n-Propyl/butyl-2-oxazoline. *Macromolecules* **2021,** *54* (23), 10667-10681.
34. Hahn, L.; Karakaya, E.; Zorn, T.; Sochor, B.; Maier, M.; Stahlhut, P.; Forster, S.; Fischer, K.; Seiffert, S.; Pöppler, A.-C.; Detsch, R.; Luxenhofer, R., An Inverse Thermogelling Bioink Based on an ABA-Type Poly(2-oxazoline) Amphiphile. *Biomacromolecules* **2021,** *22* (7), 3017-3027.
35. Bonné, T. B.; Lüdtke, K.; Jordan, R.; Štěpánek, P.; Papadakis, C. M., Aggregation behavior of amphiphilic poly(2-alkyl-2-oxazoline) diblock copolymers in aqueous solution studied by fluorescence correlation spectroscopy. *Colloid Polym. Sci.* **2004,** *282* (8), 833-843.
36. Hiller, W.; Engelhardt, N.; Kampmann, A.-L.; Degen, P.; Weberskirch, R., Micellization and Mobility of Amphiphilic Poly(2-oxazoline) Based Block Copolymers Characterized by 1H NMR Spectroscopy. *Macromolecules* **2015,** *48* (12), 4032-4045.
37. Volet, G.; Chanthavong, V.; Wintgens, V.; Amiel, C., Synthesis of Monoalkyl End-Capped Poly(2-methyl-2-oxazoline) and Its Micelle Formation in Aqueous Solution. *Macromolecules* **2005,** *38* (12), 5190-5197.
38. Dionzou, M.; Morère, A.; Roux, C.; Lonetti, B.; Marty, J.-D.; Mingotaud, C.; Joseph, P.; Goudounèche, D.; Payré, B.; Léonetti, M.; Mingotaud, A. F., Comparison of methods for the fabrication and the characterization of polymer self-assemblies: what are the important parameters? . *Soft Matter* **2016,** *12*, 2166-2176.
39. Akiba, I.; Sakurai, K., Characterizing block-copolymer micelles used in nanomedicines via solution static scattering techniques. *Polymer Journal* **2021,** *53* (9), 951-973.
40. Ghezzi, M.; Pescina, S.; Padula, C.; Santi, P.; Del Favero, E.; Cantù, L.; Nicoli, S., Polymeric micelles in drug delivery: An insight of the techniques for their characterization and assessment in biorelevant conditions. *J. Controlled Release* **2021,** *332*, 312-336.
41. Patterson, J. P.; Robin, M. P.; Chassenieux, C.; Colombani, O.; O'Reilly, R. K., The analysis of solution self-assembled polymeric nanomaterials. *Chem. Soc. Rev.* **2014,** *43*, 2412-2425.
42. Zhang, L.; Eisenberg, A., Multiple Morphologies of "Crew-Cut" Aggregates of Polystyrene-b-poly(acrylic acid) Block Copolymers. *Science* **1995,** *268* (5218), 1728-1731.